Pin potential effect on vortex pinning in YBa$_2$Cu$_3$O$_{7-\delta}$ films containing nanorods: Pin size effect and mixed pinning

Tomoya Horide iD, Naoki Matsukida, Manabu Ishimaru, Ryusuke Kita, Satoshi Awaji, and Kaname Matsumoto

View Online   Export Citation   CrossMark

ARTICLES YOU MAY BE INTERESTED IN

Isotropic enhancement in the critical current density of YBCO thin films incorporating nanoscale Y$_2$BaCuO$_5$ inclusions
Journal of Applied Physics **122**, 093905 (2017); https://doi.org/10.1063/1.5001273

Improvement in J$_c$ performance below liquid nitrogen temperature for SmBa$_2$Cu$_3$O$_y$ superconducting films with BaHfO$_3$ nano-rods controlled by low-temperature growth
APL Materials **4**, 016102 (2016); https://doi.org/10.1063/1.4939182

Influence of matching field on critical current density and irreversibility temperature in YBa$_2$Cu$_3$O$_7$ films with BaMO$_3$ (M=Zr, Sn, Hf) nanorods
Applied Physics Letters **108**, 082601 (2016); https://doi.org/10.1063/1.4942463

Pin potential effect on vortex pinning in YBa$_2$Cu$_3$O$_{7-\delta}$ films containing nanorods: Pin size effect and mixed pinning

Tomoya Horide,[1,a)] Naoki Matsukida,[1] Manabu Ishimaru,[1] Ryusuke Kita,[2] Satoshi Awaji,[3] and Kaname Matsumoto[1]

[1]*Department of Materials Science and Engineering, Kyushu Institute of Technology, 1-1 Sensui-cho, Tobata-ku, Kitakyushu 804-8550, Japan*
[2]*Graduate School of Integrated Science and Technology, Shizuoka University, 3-5-1 Johoku, Naka-ku, Hamamatsu 432-8561, Japan*
[3]*Institute for Materials Research, Tohoku University, Aoba-ku, Sendai 980-8577, Japan*

The pin size effect and mixed pinning of nanorods and matrix defects are discussed for YBa$_2$Cu$_3$O$_{7-\delta}$ films containing nanorods. BaSnO$_3$ nanorods with a diameter of 11 nm and BaHfO$_3$ nanorods with a diameter of 7 nm were prepared, and critical current density (J_c) and resistivity were measured in the films. When the coherence length was larger than the nanorod size at high temperatures near the critical temperature, the trapping angle and activation energy of the vortex flow depended on the nanorod diameter. At a moderate temperature of $65-77$ K, the pin size effect on J_c disappeared since the coherence length became smaller than the nanorod size. At a low temperature of 20 K, the contribution from matrix pinning became comparable to that of nanorods in a high magnetic field due to the small coherence length. Thus, the temperature-dependent coherence length caused the pin potential situation to vary significantly, namely, the pin size effect and mixed pinning, which strongly affected vortex pinning in YBa$_2$Cu$_3$O$_{7-\delta}$ containing nanorods. *Published by AIP Publishing.*
[http://dx.doi.org/10.1063/1.4975300]

The critical current density (J_c) is significantly improved by BaMO$_3$ (BMO; M = Zr, Sn, Hf) nanorods in YBa$_2$Cu$_3$O$_{7-\delta}$ (YBCO) films in a coated conductor application.[1] By optimizing the BMO selection and the growth conditions, a high J_c and global pinning force maximum ($F_{p,max}$) have been reported at 77 K (Ref. 2) and 4.2 K.[3] However, despite these efforts, the vortex pinning mechanism in YBCO + BMO films is not yet fully understood, and an understanding of the vortex pinning is needed for further design and control of J_c.

The nanorods act as the c-axis correlated pinning centers in the YBCO films. A pinning distribution defined by a density (spacing) and a vertical shape (nanorod length) has a significant influence on J_c, as predicted by the Bose glass theory.[4] The nanorod length along the film thickness determines the pin volume,[5] and the vortex behavior varies at the matching field.[6] Elastic strain,[7] stacking faults,[8] and oxygen vacancies[9,10] were discussed to clarify the elementary pinning force (f_p) and critical temperature (T_c). Thus, these J_c factors are becoming clearer for the YBCO + BMO films. On the other hand, the nanorod diameter depended on growth conditions and nanorod materials ($20-35$ nm;[11] $10-15$ nm;[12] $8-13$ nm;[13] $5-6$ nm (Ref. 14–16)), but the nanorod density was simultaneously varied. Since it was difficult to analyze the pin size effect separately from other factors, such as the matching field and nanorod length, the influence of the nanorod size on J_c remains unclear. Furthermore, it is unclear whether the nanorods remain dominant in the vortex pinning over other defects over a wide range of temperatures and magnetic fields. These matters are all related to the strength of the pin potential of nanorods and should be discussed for the

design and understanding of vortex pinning in YBCO films containing nanorods. In the present study, nanorod pinning is discussed in the YBCO + BMO films from the viewpoint of the pin potential. The nanorod diameter was controlled while maintaining almost the same nanorod density. The magnetic field, field angle, and temperature dependencies of J_c and the resistivity (ρ) were measured. Based on the results, the pin size effect and the mixed pinning of nanorods and matrix defects will be discussed from the viewpoint of the pin potential.

The YBCO films were prepared on SrTiO$_3$ (100) single crystalline substrates using pulsed laser deposition. YBCO + BaSnO$_3$ (BSO) (5.4 vol. %) and YBCO + BaHfO$_3$ (BHO) (3.1 vol. %) mixed targets were ablated. The film thickness was 220 nm for the YBCO + BSO (5.4) film and 190 nm for the YBCO + BHO (3.1) film. The microstructures of the films were observed using transmission electron microscopy (TEM). 1-mm long and 100–μm wide bridges were formed using the conventional photolithography and H$_3$PO$_4$ etching to measure J_c using the Physical Property Measurement System. Here, the angle between the magnetic field and the c-axis was defined as the field angle (θ). The temperature and field angle dependencies of the resistivity were measured under a current density of 50 A/cm^2 to obtain the irreversibility temperature (T_{irr}), activation energy (U_a), and trapping angle (θ_t). J_c was also measured at the High Field Laboratory for Superconducting Materials, Institute for Materials Research, Tohoku University, to evaluate the vortex pinning at a low temperature.

Figure 1 shows cross-sectional bright-field TEM images of the YBCO + BSO (5.4) and YBCO + BHO (3.1) films. Nanorods elongated along the c-axis are clearly observed in the TEM images. The diameter of the nanorods was 11 nm

a)Author to whom correspondence should be addressed. Electronic mail: horide@post.matsc.kyutech.ac.jp
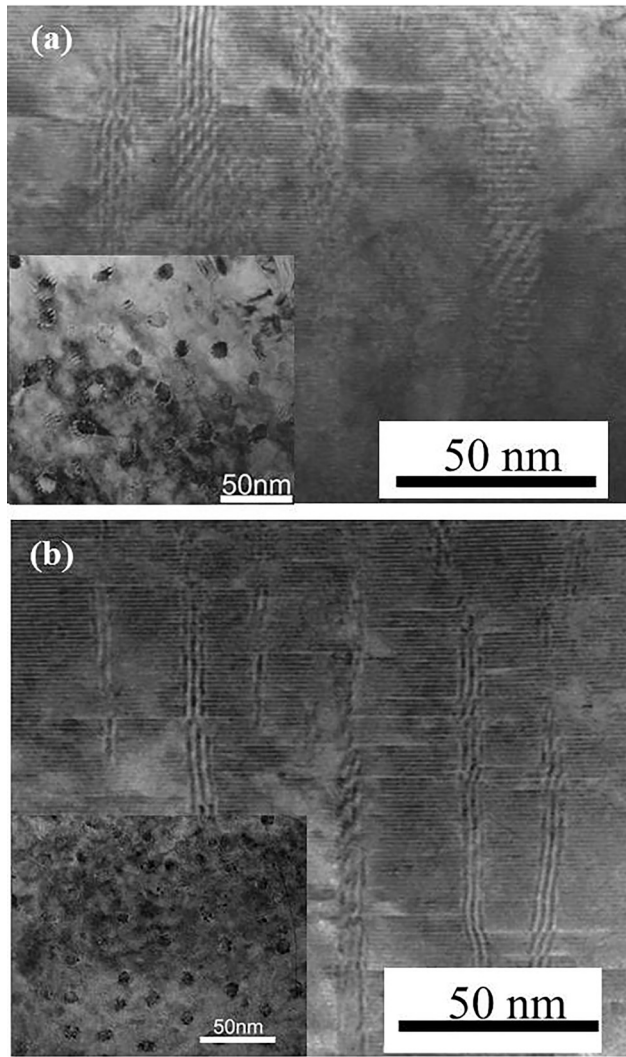
FIG. 1. Cross-sectional bright-field TEM image of (a) YBCO + BSO (5.4) and (b) YBCO + BHO (3.1) films. The insets show plane-view TEM images of the films.

for the YBCO + BSO (5.4) film and 7 nm for the YBCO + BHO (3.1) film. The plane-view TEM images are also shown in the insets of Fig. 1. A nanorod density was 9.6×10^{14} m^{-2} for the YBCO + BSO (5.4) film and 1.3×10^{15} m^{-2} for the YBCO + BHO (3.1) film. Because B_Φ is given by $n\phi_0$ (n: nanorod density, $\phi_0 = 2.07 \times 10^{-15}$ Wb [magnetic flux quantum]), B_Φ is 2.0 T for the YBCO + BSO (5.4) film and 2.6 T for the YBCO + BHO (3.1) film. Figure 2 shows the magnetic field dependence of normalized T_{irr} (T_{irr}/T_c) in the YBCO + BSO (5.4) with $T_c = 89.6$ K and YBCO + BHO (3.1) films with $T_c = 89.0$ K. A shoulder in the B–T_{irr}/T_c curves was observed at $\sim$2 T for the YBCO + BSO (5.4) film and at $\sim$3 T for the YBCO + BHO (3.1) film owing to the matching field effect. The B_Φ values estimated from the T_{irr} shoulder was consistent with those from the TEM. According to our previous paper,[6] the matching field difference in these films was too small to conceal the pin potential effect, but the "slight" difference in the matching field should not be neglected in the J_c and ρ difference between the films.

In addition to T_{irr}, the activation energy can be obtained from the temperature dependence of the resistivity, which is
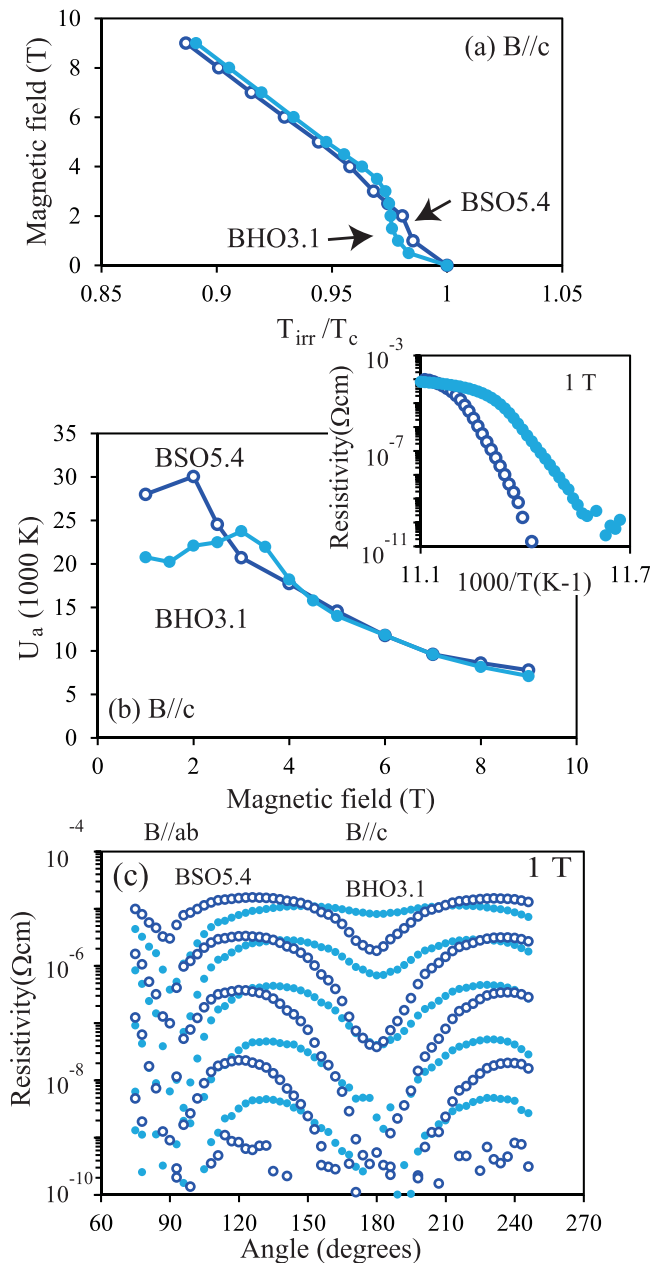

FIG. 2. (a) T_{irr}/T_c-B curves in a magnetic field parallel to the *c*-axis for the YBCO + BSO (5.4) and YBCO + BHO (3.1) films. (b) Magnetic field dependence of U_a. The inset shows the resistivity as a function of $1000/T$ at 1 T. (c) Temperature dependence of ρ-θ curve at 1 T for the YBCO + BSO (5.4) film ($T = 88.5$, 88, 87.5, 87, and 86.5 K, corresponding to $T/T_c = 0.988-0.966$) and the YBCO + BHO (3.1) film ($T = 88$, 87.5, 87, 86.5, and 86 K, corresponding to $T/T_c = 0.989-0.967$).

described by the Arrhenius relation of $\rho \sim \exp(-U_a/kT)$. Here, k is the Boltzmann constant. Figure 2(b) and its inset show the magnetic field dependence of U_a and the Arrhenius plot, respectively, indicating that U_a in the YBCO + BSO (5.4) film was 1.4 times larger than that in the YBCO + BHO (3.1) film at 1 T. The uncorrelated pinning effect is negligible near T_c due to the large coherence length, as will be discussed later, and therefore nanorod pinning should be discussed for this temperature range. Since the vortex interaction maximized nanorod pinning at the matching field, a larger U_a was obtained for the YBCO + BHO (3.1) film at its matching field of $\sim$3 T. Figure 2(c) shows the angular dependence of the resistivity at 1 T, where a dip near

$\theta = 180°$ ($B//c$) is clearly observed. Since half of the dip width corresponds to the trapping angle, the trapping angle is estimated to be 57° for the YBCO + BSO (5.4) film and 45° for the YBCO + BHO (3.1) film. The trapping angle is discussed for the same resistivity range, which corresponds to the same T/T_c range. Also, in the case of columnar defects, the trapping angle of 60°–75° depended on the samples, possibly due to differences in the diameter, as will be discussed later.[17–19] The trapping angle depends on the pin potential, as described by the following equation:[17,20]

$$\tan \theta_t = \sqrt{\frac{2U_p}{\varepsilon_l}}, \tag{1}$$

where U_p is the pinning potential of nanorods and ε_l is the line tension of the vortex. The pin potential estimated from the trapping angle is 2.4 times larger for the YBCO + BSO (5.4) film than for the YBCO + BHO (3.1) film. The dependence of the pin potential on the coherence length (ξ_{ab}) and the radius of nanorods (r) is given theoretically by following expression at the high temperature limit:[4]

$$U_p = \varepsilon_0 \left(\frac{r}{2\xi_{ab}}\right)^2. \tag{2}$$

Here, $\varepsilon_0 = \phi_0^2/4\pi\mu_0\lambda^2$, where μ_0 and λ are the permeability and the penetration depth, respectively. The pin potential ratio is 2.5 at ∼88 K, where the coherence length is ∼9 nm. The pin potential ratio experimentally obtained in Fig. 2(c) is roughly consistent with the theoretical estimation from Eq. (2). The activation energy was also varied by the influence of the nanorod size on the pin potential, as observed in Fig. 2(b). When the vortex core size is larger than the nanorods, vortices act as a "line-like" pinning center whose volume is not large enough to pin the vortex core. In this pinning situation at high temperatures near T_c, the vortex behavior strongly depends on the nanorod size.

To discuss the vortex behavior in the moderate temperature range (65−77 K), Fig. 3(a) shows the magnetic field dependencies of J_c and F_p in the films. The YBCO + BHO (3.1) and YBCO + BSO (5.4) films exhibited almost the same J_c values for a magnetic field smaller than the matching field, but the J_c for the YBCO + BHO (3.1) film was higher than that for the YBCO + BSO (5.4) film at high magnetic fields. The F_p peaks around the matching field suggest that nanorod pinning dominated J_c–B at this temperature range and the slight difference in the matching field effect resulted in the largest F_p difference ($\Delta F_p = F_p$(YBCO + BHO)−F_p (YBCO + BSO)) around B_Φ. The angular dependence of J_c at 77 K and 1 T is also shown in Fig. 3(b). The J_c–θ characteristics in the YBCO + BSO (5.4) and YBCO + BHO (3.1) films at 77 K and 1 T were almost the same, although the ρ-θ curves were significantly different between the films at 86−88 K. In particular, the J_c minimum was obtained at almost the same angle at 77 K, while the difference in the trapping angle was as large as 15° at ∼88 K. The coherence length begins to be smaller than the nanorod radius at the crossover temperature defined by $\sqrt{2}\xi(T_{r\xi}) = r$:[21] $T_{r\xi} = 80$ K at $r = 3.5$ nm for the BHO nanorods and $T_{r\xi} = 86$ K at $r = 5.5$ nm for the BSO nanorods. When the nanorod size is
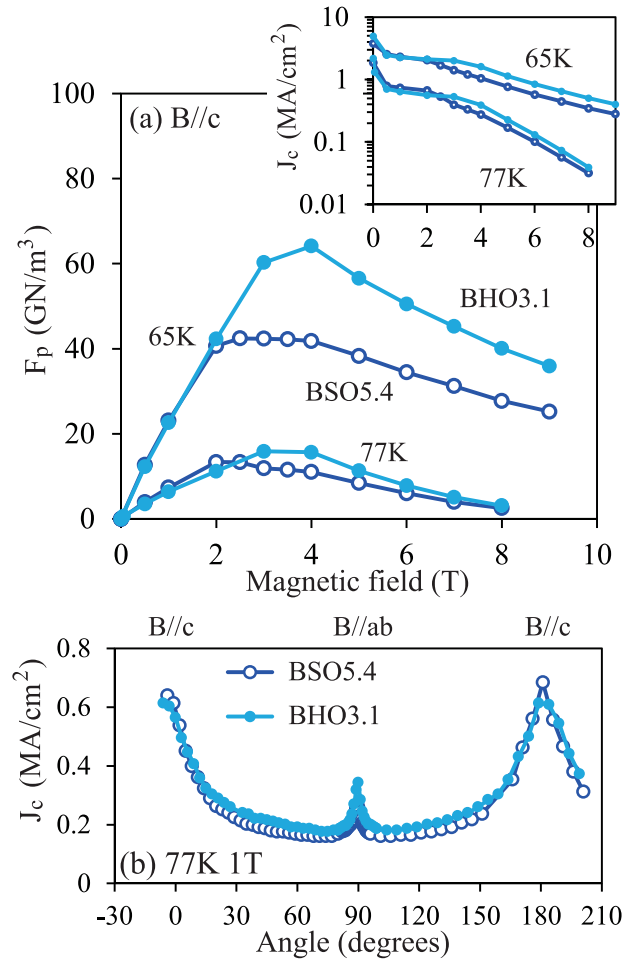

FIG. 3. (a) Magnetic field dependence of F_p at 77 and 65 K in a magnetic field parallel to the c-axis. The inset shows J_c-B curves. (b) J_c-θ curves at 1 T. Almost the same behavior was observed in the YBCO + BSO and YBCO + BHO films.

larger than the coherence length, the nanorods are "columnar" pinning centers, which can fully pin the vortex core, and it is considered that the influence of the nanorod size on the pin potential is weak. Thus, the pin size effect disappeared at the moderate temperatures and is also not expected to be observed at lower temperatures.

Figure 4(a) shows F_p as a function of the magnetic field in the films at 20 K for the discussion of an additional feature of the pin potential effect at low temperatures. F_p increased with increasing magnetic field for both films at a low magnetic field (<3 T), and the F_p behavior significantly changed at ∼3 T($\sim B_\Phi$). The nanorods are dominant to the vortex pinning at a magnetic field lower than B_Φ. On the other hand, the vortex pinning in a high magnetic field is complicated since it is determined by pinning by the matrix defects and vortex interaction. Figure 4(b) shows the J_c–θ curves in magnetic fields of 9 and 16 T at 20 K. The c-axis peaks were observed in the magnetic fields higher than the matching field for both YBCO + BSO (5.4) and YBCO + BHO (3.1) films, suggesting that the c-axis correlated pinning of nanorods affected J_c even in a high magnetic field. However, when only the nanorods are dominant, a similar F_p–B behavior is expected for the nanorods with almost the same matching field, similar to those at 65 and 77 K. On the other hand,

FIG. 5. J_c as a function of the effective field, $\varepsilon(\theta)B$, at 20 and 77 K for the YBCO + BHO (3.1) film. The lines are guides to eyes. The J_c-θ curves at 5, 9, and 16 T for 20 K and those at 1, 3, 5, 6, and 8 T for 77 K were analyzed based on the effective field.
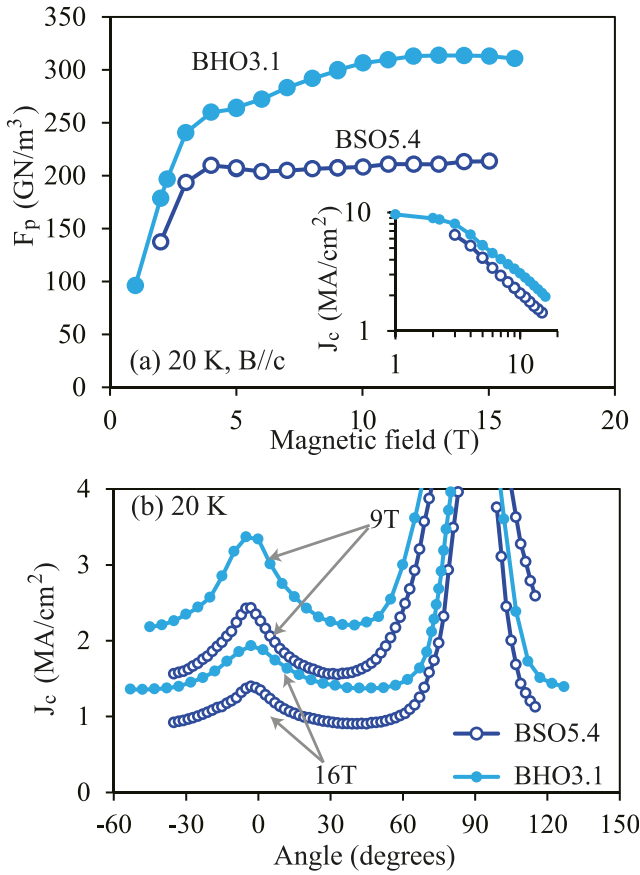

FIG. 4. (a) Magnetic field dependence of F_p for the YBCO + BHO and YBCO + BSO films at a temperature of 20 K in a magnetic field parallel to the c-axis. The inset shows a double logarithmic plot of J_c-B. (b) J_c-θ characteristics in magnetic fields of 9 and 16 T in the films at 20 K.

F_p increased with increasing magnetic field for the YBCO + BHO(3.1) film, whereas F_p was almost constant in a high magnetic field for the YBCO + BSO(5.4) film. ΔF_p was the largest at ∼15 T, which cannot be explained by nanorod pinning. To explain vortex pinning at 20 K in a high magnetic field, the mixed pinning of nanorod and matrix uncorrelated defects such as random oxygen vacancies and crystalline defects should be considered.[22] Since the pin potential of c-axis correlated pinning centers is large compared with the matrix pinning centers, vortices are trapped preferentially by the c-axis correlated pining centers. When the c-axis correlated pinning centers become occupied, vortices start to be trapped by the uncorrelated pinning centers in the matrix. Thus, it is expected that the matrix uncorrelated pinning centers affect vortex pinning mainly at high magnetic fields. Based on the effective field [$\varepsilon(\theta)B$] analysis, the J_c contribution from nanorod and matrix pinning can be discussed, where $\varepsilon(\theta) = (\cos^2\theta + \gamma^{-2}\sin^2\theta)^{1/2}$ and $\gamma = 5$.[21,23] Figure 5 shows J_c as a function of $\varepsilon(\theta)B$ at 20 and 77 K for the YBCO + BHO(3.1) film. The total J_c and J_c contributions from matrix pinning are 5.4 MA/cm^2 and 2.8 MA/cm^2, respectively, and the J_c contribution from nanorods is 2.6 MA/cm^2 at $\varepsilon(\theta)B = 5$ T for the YBCO + BHO (3.1) film. Similarly, the total J_c and the J_c contributions from matrix pinning are 4.3 MA/cm^2 and 2 MA/cm^2, respectively, and the J_c contribution from the nanorods is 2.3 MA/cm^2 at $\varepsilon(\theta)B = 5$ T for the YBCO + BSO (5.4) film (data not shown). Thus, matrix
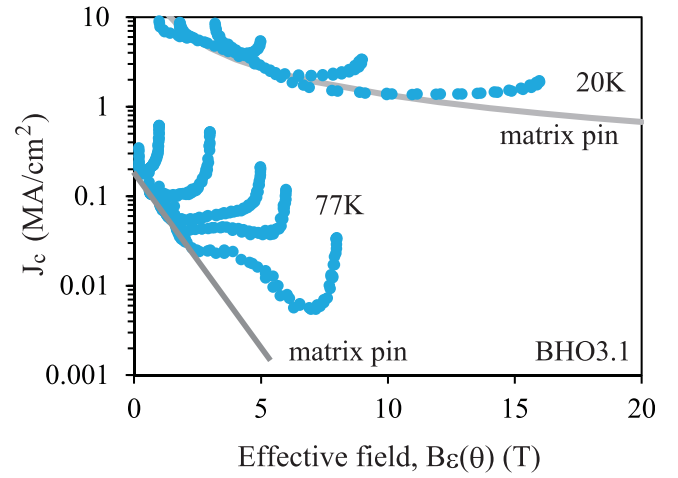
pinning and the nanorods contributed comparably to vortex pinning at 20 K, and the difference in the contribution ratio varied the J_c and F_p behavior for high magnetic fields. As for 77 K, the J_c contribution from matrix pinning is much smaller than that of the nanorods (total $J_c \sim 0.2$ MA/cm^2 at $\varepsilon(\theta)B = 5$ T and matrix contribution ∼0.02 MA/cm^2 even at $\varepsilon(\theta)B = 2$ T). Thus, matrix pinning did not significantly affect the J_c behavior at 77 K in the presence of nanorods. It was also previously reported by Gutierrez that the weak isotropic pinning contribution increased with decreasing temperature.[24] Since the coherence length is small at a low temperature, the contribution from matrix pinning is relatively strong. Thus, the mixed pinning of nanorods and matrix defects can explain both the c-axis peaks and ΔF_p–B curves at 20 K in high magnetic fields, but further studies are needed to clarify the origin of uncorrelated matrix pinning.

Based on the mixed pinning, the magnetic field dependence of J_c at 20 K will be discussed. The J_c–B curves are expressed by the power law relationship of $J_c \sim B^\alpha$. $\alpha = -1$ for the YBCO + BSO (5.4) film and $\alpha = -0.8$ for the YBCO + BHO (3.1) film at 20 K, as shown in the inset of Fig. 4(a). $\alpha = -1$ for the collective pinning by the c-axis correlated pinning,[4,21] whereas α was 0, $-1/2$, $-5/8$, and -1 depending on f_p and the pin density in the case of particle or point pinning.[25,26] In the case of mixed pinning, since J_c is determined by the summation of these effects, the α values (-1 for the YBCO + BSO film and -0.8 for the YBCO + BHO film) depended on the contribution ratio of nanorod pinning and matrix pinning.

In summary, the vortex pinning and vortex dynamics were discussed in the YBCO films containing nanorods with different diameters and almost the same density. At high temperatures, the difference in the nanorod size caused the pin potential to vary significantly, resulting in a nanorod-size dependent trapping angle and activation energy. At moderate temperatures of 65–77 K, while the pin size effect disappeared, the nanorods were still dominant in determining the vortex pinning. At a low temperature of 20 K, matrix pinning became relatively strong, and the mixed pinning of nanorods and matrix defects dominated the J_c behavior in a high

magnetic field. Thus, the pin potential situation, which depends strongly affects the vortex pinning in YBCO containing nanorods.

[1] S. R. Foltyn, L. Civale, J. L. M. Driscoll, Q. X. Jia, B. Maiorov, H. Wang, and M. Maley, Nat. Mater. **6**, 631 (2007).

[2] P. Mele, K. Matsumoto, T. Horide, A. Ichinose, M. Mukaida, Y. Yoshida, S. Horii, and R. Kita, Supercond. Sci. Technol. **21**, 032002 (2008).

[3] A. Xu, L. Delgado, N. Khatri, Y. Liu, V. Selvamanickam, D. Abraimov, J. Jaroszynski, F. Kametani, and D. C. Larbalestier, APL Mater. **2**, 046111 (2014).

[4] D. R. Nelson and V. M. Vinokur, Phys. Rev. B **48**, 13060 (1993).

[5] T. Horide, K. Matsumoto, P. Mele, Y. Yoshida, R. Kita, S. Horii, and M. Mukaida, Phys. Rev. B **79**, 092504 (2009).

[6] T. Horide, K. Taguchi, K. Matsumoto, N. Matsukida, M. Ishimaru, P. Mele, and R. Kita, Appl. Phys. Lett. **108**, 082601 (2016).

[7] T. Horide, T. Kitamura, A. Ichinose, and K. Mastumoto, Jpn. J. Appl. Phys., Part 1 **53**, 083101 (2014).

[8] A. Llordes, A. Palau, J. Gazquez, M. Coll, R. Vlad, A. Pomar, J. Arbiol, R. Guzman, S. Ye, V. Rouco, F. Sandiumenge, S. Ricart, T. Puig, M. Varela, D. Chateigner, J. Vanacken, J. Gutierrez, V. Moshchalkov, G. Deutsher, C. Magen, and X. Obradors, Nat. Mater. **11**, 329 (2012).

[9] C. Cantoni, Y. Gao, S. H. Wee, E. D. Specht, J. Gazquez, J. Meng, S. J. Pennycook, and A. Goyal, ACS Nano **5**, 4783 (2011).

[10] T. Horide and K. Matsumoto, Supercond. Sci. Technol. **27**, 115013 (2014).

[11] T. Horide, K. Matsumoto, A. Ichinose, M. Mukaida, Y. Yoshida, and S. Horii, Supercond. Sci. Technol. **20**, 303 (2007).

[12] D. M. Feldmann, T. G. Holesinger, B. Maiorov, S. R. Foltyn, J. Y. Coulter, and I. Apodaca, Supercond. Sci. Technol. **23**, 095004 (2010).

[13] S. Horii, M. Haruta, A. Ichinose, and T. Doi, J. Appl. Phys. **118**, 133907 (2015).

[14] J. Z. Wu, J. J. Shi, J. F. Baca, R. Emergo, T. J. Haudan, B. Maiorov, and T. Holesinger, Supercond. Sci. Technol. **27**, 044010 (2014).

[15] S. H. Wee, Y. L. Zuev, C. Cantoni, and A. Goyal, Sci. Rep. **3**, 2310 (2013).

[16] V. Selvamanickam, M. H. Gharahcheshmeh, A. Xu, E. Galstyan, L. Delgado, and C. Cantoni, Appl. Phys. Lett. **106**, 032601 (2015).

[17] L. M. Paulius, J. A. Fendrich, W. K. Kwok, A. E. Koshelev, V. M. Vinokur, G. W. Crabtree, and B. G. Glagola, Phys. Rev. B **56**, 913 (1997).

[18] R. J. Olsson, W. K. Kwok, L. M. Paulius, A. M. Petrean, D. J. Hofman, and G. W. Crabtree, Phys. Rev. B **65**, 104520 (2002).

[19] J. Hua, U. Welp, J. Schlueter, A. Kayani, Z. L. Xiao, G. W. Crabtree, and W. K. Kwok, Phys. Rev. B **82**, 024505 (2010).

[20] T. Horide and K. Matsumoto, Appl. Phys. Lett. **101**, 112604 (2012).

[21] G. Blatter, M. V. Feigel'man, V. B. Geshkenbein, A. I. Larkin, and V. M. Vinokur, Rev. Mod. Phys. **66**, 1125 (1994).

[22] A. Xu, V. Braccini, J. Jaronszynski, Y. Xin, and D. C. Larbalestier, Phys. Rev. B **86**, 115416 (2012).

[23] L. Civale, B. Maiorov, A. Serquis, J. O. Willis, J. Y. Coulter, H. Wang, Q. X. Jia, P. N. Arendt, J. L. MacManus-Driscoll, M. P. Maley, and S. R. Foltyn, Appl. Phys. Lett. **84**, 2121 (2004).

[24] J. Gutierrez, T. Puig, and X. Obradors, Appl. Phys. Lett. **90**, 162514 (2007).

[25] G. Blatter, V. B. Geshkenbein, and J. A. G. Koopmann, Phys. Rev. Lett. **92**, 067009 (2004).

[26] W. K. Kwok, U. Welp, A. Glatz, A. E. Koshelev, K. J. Kihlstrom, and G. W. Crabtree, Rep. Prog. Phys. **79**, 116501 (2016).